# Electron-optical-phonon scattering rates in a rectangular semiconductor quantum wire

K. W. Kim
*Department of Electrical and Computer Engineering, North Carolina State University, Raleigh, North Carolina 27695-7911*

M. A. Stroscio
*U. S. Army Research Office, P. O. Box 12211, Research Triangle Park, North Carolina 27709-2211*

A. Bhatt
*Department of Electrical and Computer Engineering, North Carolina State University, Raleigh, North Carolina 27695-7911*

R. Mickevicius and V. V. Mitin
*Department of Electrical and Computer Engineering, Wayne State University, Detroit, Michigan 48202*

(Received 6 February 1991; accepted for publication 2 April 1991)

One-dimensional electron-optical-phonon interaction Hamiltonians in a rectangular quantum wire consisting of diatomic polar semiconductors are derived under the macroscopic dielectric continuum model. The scattering rates calculated in a GaAs square quantum wire show that when the quantum wire is free-standing in vacuum, the interaction by the surface-optical phonon modes is very strong and may dominate over other scattering processes, especially with dimensions of about 100 Å or less. When the wire is embedded in a polar semiconductor (AlAs to be specific), the scattering rates by the surface-optical phonon modes become generally smaller, but yet comparable to those by the confined longitudinal-optical modes as the wire dimension shrinks. A considerable decrease in the total scattering rate for optical phonons as a result of simple reduction in dimensionality is not observed in this study.

## I. INTRODUCTION

Recent advances in epitaxial growth technology for compound semiconductor structures have made possible the fabrication of wire-like regions of narrow-band-gap semiconductor material surrounded completely by regions of large-band-gap semiconductor material. In particular, such wire-like structures have been fabricated with rectangular cross sections having dimensions small relative to the electron thermal de Broglie wavelength; furthermore, optical anisotropy measurements on these wire-like structures provide evidence of two-dimensional quantum confinement of charge carriers.[1] In such structures, the electron-optical-phonon scattering rate is affected by changes in the Fröhlich interaction Hamiltonian caused by phonon confinement and localization as well as by changes in the wave functions of the charge carriers due to the confining rectangular potential. The presence of heterointerfaces gives rise to the confinement of optical phonons in each layer (i.e., confined modes) and the localization in the vicinity of interfaces (i.e., surface modes or interface modes). Indeed, recent measurements have provided striking evidence of surface-optical (SO) modes in cylindrical quantum wires[2] and phonon confinement.[3] The effects of carrier confinement on the total scattering rates for polar-optical-phonon scattering in quantum wells and quantum wires have been evaluated previously by Leburton[4] with bulk longitudinal-optical (LO) phonon modes.

In this paper, one-dimensional (1D) electron-optical-phonon scattering rates in rectangular quantum wires (with diatomic binary polar semiconductors) are determined not only by including the effects of carrier confinement but also by replacing bulk LO-phonon modes with appropriate optical-phonon modes for a 1D system (i.e., the confined LO-phonon and SO-phonon modes). The results demonstrate that electron-SO-phonon scattering can be strong and may dominate over (or, at least, be comparable to) other scattering processes in ultrasmall quantum-wire structures[1,2] and in mesoscopic structures[5] containing wire-like regions of polar semiconductors. Thus, it is expected that a simple reduction in dimensionality may not cause a significant decrease in the total scattering rate for optical phonons in rectangular quantum-wire structures. On the other hand, this finding does not preclude the possibility of dramatical reduction in optical-phonon scattering by appropriate tailoring of electronic bandstructure, as suggested by Sakaki.[6] The rest of this paper is organized as follows. Section II briefly summarizes the derivation of interaction Hamiltonian for confined LO-phonon modes in a rectangular quantum wire. Section III describes the characteristic SO-phonon modes and the interaction Hamiltonian. Finally, Sec. IV presents the total electron-optical-phonon scattering rate in quantum wires of various dimensions and identifies the separate contributions of SO and LO scattering rates.

## II. INTERACTION HAMILTONIAN FOR LO PHONONS CONFINED IN A RECTANGULAR QUANTUM WIRE

Licari and Evrard[7] have calculated the operators describing the interaction between an electron and the opti-

 0021-8979/91/010319-09$03.00  

cal-phonon modes of an ionic crystal slab and have derived explicit expressions for the confined LO modes and the SO modes for such a slab. Furthermore, it was shown that the interaction operator for confined LO modes is, indeed, equivalent to the Fröhlich Hamiltonian for bulk LO phonons in the limit as the slab becomes very thick. A similar and more comprehensive treatment of the electron-optical-phonon interaction in single and double heterostructures (i.e., quantum wells) has been given by Mori and Ando.[8] To derive the Fröhlich Hamiltonian describing the interaction of confined LO phonons and electrons in a quantum-wire structure as shown in Fig. 1(a), the three-dimensional Fröhlich operator is subjected to appropriate boundary conditions in both the $y$ direction and the $z$ direction. Following an approach based on the macroscopic continuum model with electrostatic boundary conditions (similar to Licari and Evrard[7] and Mori and Ando[8]), Stroscio[9] has developed an expression for the interaction Hamiltonian for confined LO-phonon modes in a rectangular quantum wire:

$$
\begin{aligned}
H_{\mathrm{LO}}^{(1\mathrm{D})}=2\alpha' \sum_{k_x} e^{ik_x x}\Bigg\{ & \sum_{m=1,3,5,\ldots}\sum_{n=1,3,5,\ldots} \frac{\cos\left(\frac{m\pi}{L_y}y\right)\cos\left(\frac{n\pi}{L_z}z\right)}{\left[k_x^2+\left(\frac{m\pi}{L_y}\right)^2+\left(\frac{n\pi}{L_z}\right)^2\right]^{1/2}}\left[A(k_x)+A^{\dagger}(-k_x)\right] \\
& + \sum_{m=1,3,5,\ldots}\sum_{n=2,4,6,\ldots} \frac{\cos\left(\frac{m\pi}{L_y}y\right)\sin\left(\frac{n\pi}{L_z}z\right)}{\left[k_x^2+\left(\frac{m\pi}{L_y}\right)^2+\left(\frac{n\pi}{L_z}\right)^2\right]^{1/2}}\left[A(k_x)+A^{\dagger}(-k_x)\right] \\
& + \sum_{m=2,4,6,\ldots}\sum_{n=1,3,5,\ldots} \frac{\sin\left(\frac{m\pi}{L_y}y\right)\cos\left(\frac{n\pi}{L_z}z\right)}{\left[k_x^2+\left(\frac{m\pi}{L_y}\right)^2+\left(\frac{n\pi}{L_z}\right)^2\right]^{1/2}}\left[A(k_x)+A^{\dagger}(-k_x)\right] \\
& + \sum_{m=2,4,6,\ldots}\sum_{n=2,4,6,\ldots} \frac{\sin\left(\frac{m\pi}{L_y}y\right)\sin\left(\frac{n\pi}{L_z}z\right)}{\left[k_x^2+\left(\frac{m\pi}{L_y}\right)^2+\left(\frac{n\pi}{L_z}\right)^2\right]^{1/2}}\left[A(k_x)+A^{\dagger}(-k_x)\right]\Bigg\}, \qquad (1)
\end{aligned}
$$

where $\alpha'=\{(e^2/2\epsilon_o L_y L_z L)\hbar\omega_{l1}[1/\epsilon_1(\infty)-1/\epsilon_1(0)]\}^{1/2}$, $\epsilon_o$ is the permittivity of vacuum, $\epsilon_1(\infty)$ and $\epsilon_1(0)$ are the high- and low-frequency dielectric constants in the quantum wire (material 1), $m$ and $n$ are the phonon mode numbers in the $y$ and $z$ directions, respectively, $k_x$ is the phonon wave vector in the direction of free propagation, and $A$ and $A^{\dagger}$ represent the appropriate phonon annihilation and creation operators. In Eq. (1), electrons and the LO-phonon modes are characterized as traveling waves in the $x$ direction and standing waves in the $y$ and $z$ directions. The change in the frequency of confined LO-phonon mode[10] in the quantum wire, $\omega_{l1}$, is not considered. For proper normalization throughout this paper, the volume of the whole structure (including the region with material 2) is assumed to be $L^3$ (i.e., $-L/2 \leqslant x,y,z \leqslant L/2$, $L_y \ll L$, $L_z \ll L$) with periodic boundary conditions.

## III. SO-PHONON MODES IN A RECTANGULAR QUANTUM WIRE

In this section, the polarization eigenvectors and dispersion relations for SO-phonon modes are derived in the continuum approximation. The results presented herein are more general than those reported previously,[11] in which a quantum wire was assumed to be free-standing in vacuum (i.e., $\epsilon_2=1$ and no polarization for the material outside of the quantum wire). Instead, the quantum wire with a dielectric function $\epsilon_1(\omega)$ is taken to be surrounded by a material with a dielectric function $\epsilon_2(\omega)$ as shown in Fig. 1(a). The Lyddane–Sachs–Teller relation is assumed for the frequency dependence of the dielectric function in material $n$, $\epsilon_n(\omega)$. Since the system is translationally invariant in the $x$ direction, the potential describing the optical-phonon modes may be taken as

$$\Phi(\mathbf{r})=\sum_{k_x}\Phi(k_x,y,z)e^{ik_x x}, \qquad (2)$$

where $k_x$ is the phonon wave vector in the $x$ direction. In the absence of any free charge, the divergence of the displacement vector must vanish and it follows that the potential $\Phi(k_x,y,z)$ of the SO-phonon modes must satisfy

$$\epsilon_n(\omega)\left(\frac{\partial^2}{\partial y^2}+\frac{\partial^2}{\partial z^2}-k_x^2\right)\Phi(k_x,y,z)=0, \qquad (3)$$

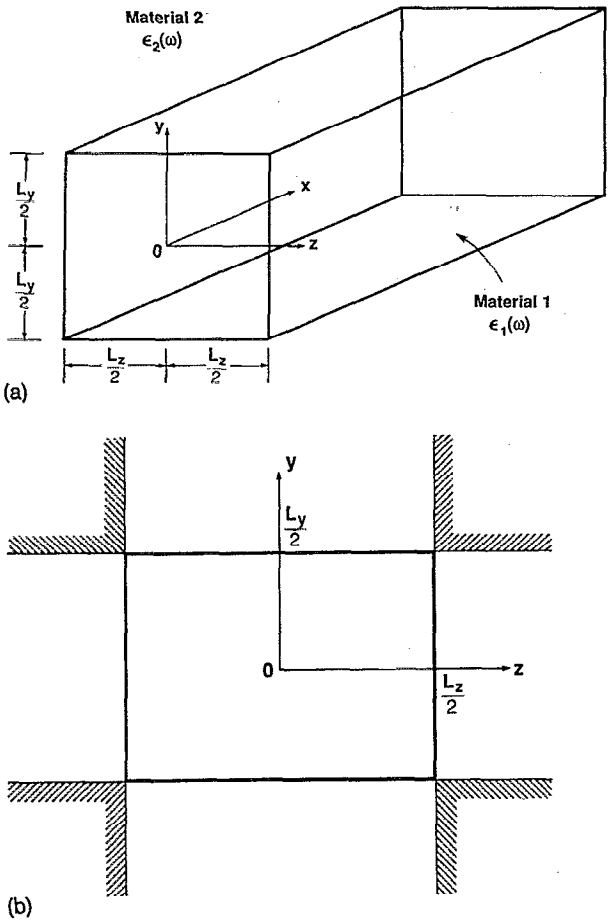


FIG. 1. (a) Schematic representation of a rectangular quantum wire with material 1 (inside) surrounded by material 2 (outside). $\epsilon_1(\omega)$ [$\epsilon_2(\omega)$] is the dielectric function for material 1 (2), respectively. (b) Cross-sectional view of the quantum-wire structure used to model the characteristic SO-phonon modes.

with $\epsilon_n(\omega)\neq 0$. The derivation of Eq. (3) is straightforward upon taking the relations

$$\mathbf{E}(\mathbf{r})=\sum_{k_x}\mathbf{E}(k_x,y,z)e^{ik_x x}=-\nabla\Phi(\mathbf{r}), \tag{4}$$

$$\mathbf{P}(\mathbf{r})=\sum_{k_x}\mathbf{P}(k_x,y,z)e^{ik_x x}=\epsilon_o\chi_n(\omega)\mathbf{E}(\mathbf{r}), \tag{5}$$

with $\Phi(\mathbf{r})$ as given by Eq. (2), and where $\mathbf{E}(\mathbf{r})$ is the electric field, $\mathbf{P}(\mathbf{r})$ is the polarization field, and $\chi_n(\omega)=\epsilon_n(\omega)-1$ is the dielectric susceptibility of material $n$; a similar treatment has been used previously to arrive at the corresponding result for a quantum well.[7,8] The solutions of Eq. (3) with electrostatic boundary conditions constitute the appropriate potential for SO-phonon modes. Unlike in quantum wells, however, this boundary value problem does not have analytical solutions in rectangular quantum-wire structures. As a result, an approximation has been made to simplify the problem: i.e., while the potential $\Phi$ is kept continuous throughout the space and the normal component of $\epsilon_n\mathbf{E}$ is kept continuous at the quantum-wire boundaries as they should be, the electric field $\mathbf{E}$ is not required to properly match along the edge of shaded regions as shown in Fig. 1(b). This simplification stems from the consideration that due to the exponential decay of fields away from the quantum wire, the relaxation of boundary conditions in the shaded regions would bring only a small error in the calculation of fields and even a smaller error for the potential inside the quantum wire. A similar approach has been applied to the dielectric rectangular waveguide and has shown a remarkable accuracy.[12,13] With this assumption, Eq. (3) has a symmetric solution of the form

$$\Phi_S(k_x,y,z)=\begin{cases} C\dfrac{\cosh(\alpha y)}{\cosh(\alpha L_y/2)}\dfrac{\cosh(\beta z)}{\cosh(\beta L_z/2)}, & |y|<L_y/2,|z|<L_z/2,\\ C\dfrac{\cosh(\alpha y)}{\cosh(\alpha L_y/2)}e^{\beta L_z/2}e^{-\beta|z|}, & |y|<L_y/2,|z|>L_z/2,\\ C\,e^{\alpha L_y/2}e^{-\alpha|y|}\dfrac{\cosh(\beta z)}{\cosh(\beta L_z/2)}, & |y|>L_y/2,|z|<L_z/2,\\ C\,e^{\alpha L_y/2}e^{-\alpha|y|}e^{\beta L_z/2}e^{-\beta|z|}, & |y|>L_y/2,|z|>L_z/2, \end{cases} \tag{6}$$

and an antisymmetric solution

$$\Phi_A(k_x,y,z)=\begin{cases} C\dfrac{\sinh(\alpha y)}{\sinh(\alpha L_y/2)}\dfrac{\sinh(\beta z)}{\sinh(\beta L_z/2)}, & |y|<L_y/2,|z|<L_z/2,\\ -C\dfrac{\sinh(\alpha y)}{\sinh(\alpha L_y/2)}e^{\beta L_z/2}e^{-\beta|z|}, & |y|<L_y/2,|z|>L_z/2,\\ -C\,e^{\alpha L_y/2}e^{-\alpha|y|}\dfrac{\sinh(\beta z)}{\sinh(\beta L_z/2)}, & |y|>L_y/2,|z|<L_z/2,\\ \pm C\,e^{\alpha L_y/2}e^{-\alpha|y|}e^{\beta L_z/2}e^{-\beta|z|}, & |y|>L_y/2,|z|>L_z/2, \end{cases} \tag{7}$$

where $\alpha$ and $\beta$ satisfy the relation

$$\alpha^2+\beta^2-k_x^2=0. \tag{8}$$

The $\pm$ sign in Eq. (7) is chosen $+$ when $yz>0$ and $-$ when $yz<0$, respectively. The dispersion relation required by the boundary conditions is

$$\epsilon_1(\omega)\tanh(\alpha L_y/2)+\epsilon_2(\omega)=0, \tag{9a}$$

for the symmetric solution and

$$\epsilon_1(\omega)\coth(\alpha L_y/2)+\epsilon_2(\omega)=0, \tag{9b}$$

for the antisymmetric solution, respectively, along with the relation

$$\alpha L_y=\beta L_z, \tag{10}$$

for both Eqs. (9a) and (9b). The polarization eigenvectors for the symmetric and antisymmetric modes may be obtained from Eqs. (4)–(7).

To complete the derivation of the interaction Hamiltonian for the SO modes, it is necessary to determine the normalization constant $C$ of Eqs. (6) and (7). As in the case of a quantum well,[8,14] the microscopic relations which govern the equation of ionic motion yield the polarization field $\mathbf{P}(\mathbf{r})$ as

$$\mathbf{P}(\mathbf{r})=n_n e_n^*\Theta_n^{-1/2}\mathbf{u}(\mathbf{r})=n_n e_n^*\Theta_n^{-1/2}\sum_{k_x}\mathbf{u}(k_x,y,z)e^{ik_x x}, \tag{11}$$

where $\mathbf{u}(\mathbf{r})$ is the relative displacement of an ion pair (i.e., unit cell), $e_n^*$ is the effective charge of an ion pair, and $n_n$ is the number of ion pairs per unit volume. In addition, $\Theta_n^{-1/2}=1+\mu_n a_n(\omega^2-\omega_{on}^2)/e_n^{*2}$ where $\mu_n$ is the reduced mass of the ion pair, $a_n$ is the electronic polarizability per ion pair, and $\omega_{on}$ is the frequency associated with the short-range force between ions. To ensure proper quantization of the phonon field,[8,14] each mode must satisfy

$$\int_{-L/2}^{+L/2}dy\int_{-L/2}^{+L/2}dz[(\mu_n n_n L)^{1/2}\mathbf{u}(k_x,y,z)]^*\cdot[(\mu_n n_n L)^{1/2}\mathbf{u}(k_x,y,z)]=1. \tag{12}$$

Using the relation

$$\frac{\epsilon_o^2\chi_n^2}{n_n^2 e_n^{*2}\Theta_n^{-1}}n_n\mu_n=\epsilon_o\epsilon_n(\infty)\frac{(\omega_{ln}^2-\omega_{tn}^2)}{(\omega^2-\omega_{tn}^2)^2}=\epsilon_o\frac{1}{2\omega}\frac{\partial\epsilon_n(\omega)}{\partial\omega}, \tag{13}$$

as in Ref. 14, it follows straightforwardly from Eqs. (6), (11), and (12) that the normalization constant, $C$, for the symmetric mode satisfies,

$$\begin{aligned}L^{-1}C^{-2}=&\epsilon_o\epsilon_1(\infty)\frac{(\omega_{l1}^2-\omega_{t1}^2)}{(\omega^2-\omega_{t1}^2)^2}\left[\cosh\left(\frac{\alpha L_y}{2}\right)\cosh\left(\frac{\beta L_z}{2}\right)\right]^{-2}\left[\frac{\alpha^2}{2}\left(\frac{L_z}{\alpha}\sinh(\alpha L_y)+\frac{\sinh(\alpha L_y)\sinh(\beta L_z)}{\alpha\beta}\right)\right.\\&\left.+\frac{\beta^2}{2}\left(\frac{L_y}{\beta}\sinh(\beta L_z)+\frac{\sinh(\alpha L_y)\sinh(\beta L_z)}{\alpha\beta}\right)\right]+\epsilon_o\epsilon_2(\infty)\frac{(\omega_{l2}^2-\omega_{t2}^2)}{(\omega^2-\omega_{t2}^2)^2}\left[\cosh\left(\frac{\alpha L_y}{2}\right)\right]^{-2}\\&\times\left[\alpha^2\left(\frac{\sinh(\alpha L_y)}{\alpha\beta}\right)+\beta^2\left(\frac{\sinh(\alpha L_y)}{\alpha\beta}+\frac{L_y}{\beta}\right)\right]+\epsilon_o\epsilon_2(\infty)\frac{(\omega_{l2}^2-\omega_{t2}^2)}{(\omega^2-\omega_{t2}^2)^2}\left[\cosh\left(\frac{\beta L_z}{2}\right)\right]^{-2}\\&\times\left[\alpha^2\left(\frac{\sinh(\beta L_z)}{\alpha\beta}+\frac{L_z}{\alpha}\right)+\beta^2\left(\frac{\sinh(\beta L_z)}{\alpha\beta}\right)\right]+\epsilon_o\epsilon_2(\infty)\frac{(\omega_{l2}^2-\omega_{t2}^2)}{(\omega^2-\omega_{t2}^2)^2}\left[\frac{2(\alpha^2+\beta^2)}{\alpha\beta}\right],\end{aligned} \tag{14}$$

where the subscript $t$ represents the transverse-optical (TO) modes. A similar expression for the antisymmetric mode may be obtained straightforwardly from Eqs. (7), (11)–(13). When the quantum wire is free-standing, only the first term with $\epsilon_1$ [out of four terms in Eq. (14)] contributes to the normalization constant $C$. Finally, the interaction Hamiltonian for the SO modes may be written as

$$H_{SO}^{(1D)}=\sum_{k_x}(-e)\Phi(k_x,y,z)e^{ik_x x}\left(\frac{\hbar}{2\omega}\right)^{1/2}\times[A_{SO}(k_x)+A_{SO}^{\dagger}(-k_x)], \tag{15}$$

where $A_{SO}(k_x)$ and $A_{SO}^{\dagger}(-k_x)$ are the annihilation and creation operators for appropriate SO-phonon modes of the quantum wire.

## IV. SCATTERING RATES FOR ELECTRON-OPTICAL-PHONON INTERACTIONS

The 1D Fröhlich Hamiltonian of Eq. (1) (i.e., confined LO phonons) and the SO-phonon Hamiltonian of Eq. (15) lead to especially simple scattering matrix elements when the electronic states are confined in an infinitely deep potential well in the $y$ and $z$ directions. While treatments with more realistic confining potentials are available for LO phonons described by the three-dimensional Fröhlich Hamiltonian,[4] they generally involve the extensive applica-

tion of numerical techniques. In the present treatment, electron-optical-phonon scattering rates will be calculated with an assumption that the quantum wire forms an infinitely deep potential well and only the lowest subband is occupied (i.e., only the intra-subband scattering in the ground state is considered). However, more accurate results with the realistic conditions such as finite potentials and inter-subband scattering can be readily obtained using Eqs. (1) and (15) with numerical means.

For the infinite well potential, the ground-state 1D electron wave function has the well-known form

$$|q_x\rangle=\frac{e^{iq_x x}}{L^{1/2}}\left(\frac{2}{L_y}\right)^{1/2}\cos\left(\frac{\pi y}{L_y}\right)\left(\frac{2}{L_z}\right)^{1/2}\cos\left(\frac{\pi z}{L_z}\right). \tag{16}$$

The corresponding electron energy is

$$E(q_x)=\frac{\hbar^2 q_x^2}{2m^*}+\frac{\hbar^2}{2m^*}\left[\left(\frac{\pi}{L_y}\right)^2+\left(\frac{\pi}{L_z}\right)^2\right]. \tag{17}$$

Assuming that the Fermi golden rule gives an accurate evaluation of the probability of making a transition from an initial electronic state $q_x$ to a final electronic state $q_x'$, the transition probability is

$$W_a^{\{e\}}(q_x,q_x')=\left(\frac{2\pi}{\hbar}\right)|M_a^{\{e\}}|^2\delta[E(q_x')-E(q_x)\pm\hbar\omega], \tag{18}$$

where $e$ stands for emission, $a$ stands for absorption, the upper (lower) sign in the $\delta$ function corresponds to emission (absorption), and $M^{\{a\}}$ is the matrix element for electron-optical-phonon interaction

$$M_a^{\{e\}}=\langle q_x',N_{k_x}+\tfrac{1}{2}\pm\tfrac{1}{2}|H^{(1D)}|q_x,N_{k_x}+\tfrac{1}{2}\pm\tfrac{1}{2}\rangle. \tag{19}$$

In Eq. (19), $H^{(1D)}$ is the total electron-optical-phonon interaction Hamiltonian for a 1D quantum wire. The phonon occupation number is taken as $N_{k_x}+1$ for emission and as $N_{k_x}$ for absorption. For the interaction of electrons with confined LO-phonon modes, the transition rate $1/\tau_{LO}^{\{e\}}(q_x)$ [$=\int dk_x(L/2\pi)W_{LO}^{\{e\}}$] becomes

$$\frac{1}{\tau_{LO}^{\{e\}}(q_x)}=\int_{-\infty}^{+\infty}dk_x\frac{e^2}{8\pi^2\epsilon_o}\omega_{l1}\left(N_{k_x}+\frac{1}{2}\pm\frac{1}{2}\right)\times I_{LO}(k_x,L_y,L_z)\delta[E(q_x\pm k_x)-E(q_x)\pm\hbar\omega], \tag{20}$$

where

$$I_{LO}(k_x,L_y,L_z)=\left(\frac{1}{\epsilon_1(\infty)}-\frac{1}{\epsilon_1(0)}\right)\frac{(2\pi)^2}{L_yL_z}\times\left\{\sum_{m=1,3,5\ldots}\sum_{n=1,3,5\ldots}\frac{4P_{mn}}{\left[k_x^2+\left(\frac{m\pi}{L_y}\right)^2+\left(\frac{n\pi}{L_z}\right)^2\right]^{1/2}}\right\}^2 \tag{21}$$

and the nonvanishing $P_{mn}$ results from the first term of Eq. (1):

$$P_{mn}=\int_{-L_y/2}^{+L_y/2}\frac{dy}{(L_y/2)}\int_{-L_z/2}^{+L_z/2}\frac{dz}{(L_z/2)}\cos^2\left(\frac{\pi y}{L_y}\right)\times\cos^2\left(\frac{\pi z}{L_z}\right)\cos\left(\frac{m\pi}{L_y}y\right)\cos\left(\frac{n\pi}{L_z}z\right). \tag{22}$$

Since the dominant contribution to the sum over phonon modes is made by the mode with $m=n=1$ ($P_{11}=(8/3\pi)^2$), Eq. (21) may be approximated as

$$I_{LO}(k_x,L_y,L_z)\approx\left(\frac{1}{\epsilon_1(\infty)}-\frac{1}{\epsilon_1(0)}\right)\frac{(2\pi)^2}{L_yL_z}\times\frac{16(8/3\pi)^4}{\left[k_x^2+\left(\frac{\pi}{L_y}\right)^2+\left(\frac{\pi}{L_z}\right)^2\right]^2}. \tag{23}$$

It is important to note that the definition of $I_{LO}$ in this paper does not follow the convention of Refs. 4 and 9 in that Eqs. (21) and (23) incorporate the factor $1/\epsilon_1(\infty)-1/\epsilon_1(0)$. This change makes the comparison with the SO-phonon scattering results easier as will be discussed later.

Defining $C'$ and $\phi(k_x,y,z)$ as

$$\Phi(k_x,y,z)=C\phi(k_x,y,z)=\frac{C'}{\sqrt{\epsilon_o L}}\phi(k_x,y,z) \tag{24}$$

from Eqs. (6), (7), and (14), the transition probability (from a ground state to a ground state) by a SO-phonon interaction may be written as

$$W_{SO}^{\{e\}}(q_x,q_x')=\left(\frac{2\pi}{\hbar}\right)e^2\left(\frac{\hbar}{2\omega}\right)\frac{C'^2}{\epsilon_o L}\left[\int_{-L_y/2}^{+L_y/2}\frac{dy}{L_y/2}\int_{-L_z/2}^{+L_z/2}\frac{dz}{L_z/2}\times\phi(k_x,y,z)\cos^2\left(\frac{\pi y}{L_y}\right)\cos^2\left(\frac{\pi z}{L_z}\right)\right]^2\times\delta[E(q_x')-E(q_x)\pm\hbar\omega]\delta(q_x'-q_x\pm k_x). \tag{25}$$

For the antisymmetric SO-phonon modes, the transition probability $W_{SO}^{\{e\}}$ becomes zero when only the lowest subband is occupied as in Eq. (25) but will, in general, be nonzero when excited electronic states are considered. Taking $\phi(k_x,y,z)$ from Eq. (6), the scattering rate $1/\tau_{SO}^{\{e\}}(q_x)$ for each of symmetric SO-phonon modes, $\omega$, which satisfies Eqs. (9a) and (10) may be expressed as

$$\frac{1}{\tau_{SO}^{\{e\}}(q_x)}=\int_{-\infty}^{+\infty}dk_x\frac{e^2}{8\pi^2\epsilon_o}\omega\left(N_{k_x}+\frac{1}{2}\pm\frac{1}{2}\right)\times I_{SO}(k_x,L_y,L_z)\delta[E(q_x\pm k_x)-E(q_x)\pm\hbar\omega], \tag{26}$$

where

$$I_{SO}(k_x,L_y,L_z)=\frac{(2\pi)^2C'^2}{\omega^2}P_S^2, \tag{27}$$

and

$$P_S=\frac{1}{\cosh(\alpha L_y/2)\cosh(\beta L_z/2)}\int_{-L_y/2}^{+L_y/2}\frac{dy}{(L_y/2)}$$
$$\times\int_{-L_z/2}^{+L_z/2}\frac{dz}{(L_z/2)}\cos^2\left(\frac{\pi y}{L_y}\right)\cos^2\left(\frac{\pi z}{L_z}\right)$$
$$\times\cosh(\alpha y)\cosh(\beta z)$$
$$=\frac{1}{\cosh(\alpha L_y/2)\cosh(\beta L_z/2)}$$
$$\times\frac{4\sinh(\alpha L_y/2)\sinh(\beta L_z/2)}{(\alpha\beta L_y L_z)\left[\left(\frac{\alpha L_y}{2\pi}\right)^2+1\right]\left[\left(\frac{\beta L_z}{2\pi}\right)^2+1\right]}. \tag{28}$$

Since the formulation of Eq. (26) is identical to that of Eq. (20), direct comparison between $I_{LO}$ and $I_{SO}$ is plausible as mentioned previously. Considering the energy-conserving delta function in Eq. (26) (for the symmetric SO modes) and in Eq. (20) (for the LO modes), the expression for the scattering rate may be further simplified. Only two values of $k_x, k_{\pm}^{\{e\}}$, contribute to the integral in either the case of emission or absorption; i.e., for emission,

$$k_{\pm}^{\{e\}}=q_x\pm[q_x^2-(2m^*\omega/\hbar)]^{1/2} \tag{29a}$$

and, for absorption,

$$k_{\pm}^{\{a\}}=-q_x\pm[q_x^2+(2m^*\omega/\hbar)]^{1/2}. \tag{29b}$$

Thus, integrating Eqs. (20) or (26) over $k_x$ yields

$$\frac{1}{\tau_{|a|}^{|e|}(q_x)}=\sum_{k_x=k_+^{\{e\}},k_-^{\{e\}}}\frac{1}{2\pi}\frac{e^2m^{*1/2}\omega}{4\pi\epsilon_o\hbar\sqrt{2}}\left(N_{k_x}+\frac{1}{2}\pm\frac{1}{2}\right)$$
$$\times\frac{I(k_x,L_y,L_z)}{\sqrt{E_x(q_x)-\pm\hbar\omega}} \tag{30}$$

for each of the appropriate branches of $\omega$ with $E_x(q_x)=\hbar^2q_x^2/2m^*$.

As a specific structure in this paper, a GaAs square quantum wire of size $d$ (i.e., $L_y=L_z=d$) is chosen with two different surrounding materials. The first case deals with the GaAs quantum wire free-standing in vacuum [i.e., $\epsilon_2(\omega)=1$] and, in the second case, the wire is assumed to be embedded in AlAs (i.e., the GaAs/AlAs structure). The relevant material parameters used in the calculations are $\omega_{l1}=36.2$ meV, $\omega_{t1}=33.3$ meV, and $\epsilon_1(\infty)=10.9$ for GaAs, and $\omega_{l2}=50.1$ meV, $\omega_{t2}=44.8$ meV, and $\epsilon_2(\infty)=8.16$ for AlAs. The frequencies of symmetric and antisymmetric SO-phonon modes in both quantum-wire structures are shown in Fig. 2 as a function of $k_xd$. The results are similar to those obtained in quantum-well structures.[8,15] For the free-standing wire, one symmetric mode $\omega_{S,f}$ and one antisymmetric mode $\omega_{A,f}$ are the solutions of

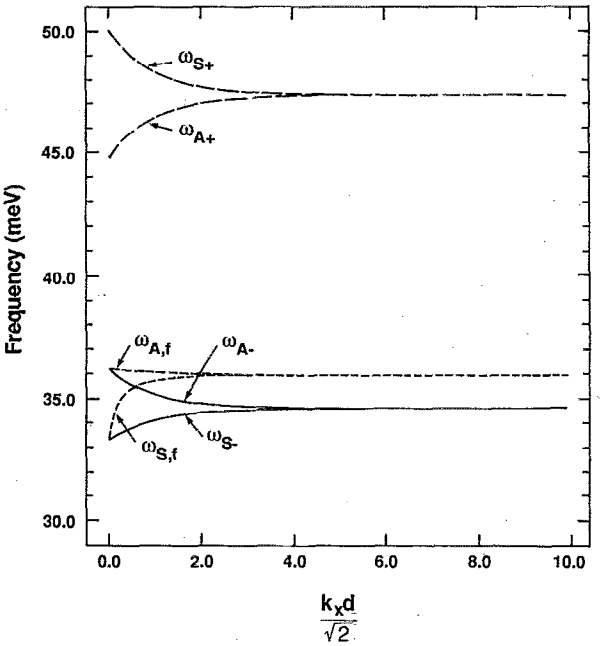


FIG. 2. Frequencies of symmetric ($\omega_{S,f},\omega_{S\pm}$) and antisymmetric ($\omega_{A,f},\omega_{A\pm}$) SO-phonon modes in a GaAs rectangular quantum wire with $L_y=L_z=d$. While $\omega_{S,f}$ and $\omega_{A,f}$ are for the wire free-standing in the vacuum, $\omega_{S\pm}$ and $\omega_{A\pm}$ are for the wire embedded in AlAs.

Eqs. (9a) and (9b), respectively, while the GaAs/AlAs structure (embedded in AlAs) exhibits two characteristic frequencies for the symmetric modes ($\omega_{S\pm}$) and the antisymmetric modes ($\omega_{A\pm}$). As can be seen in the figure, the

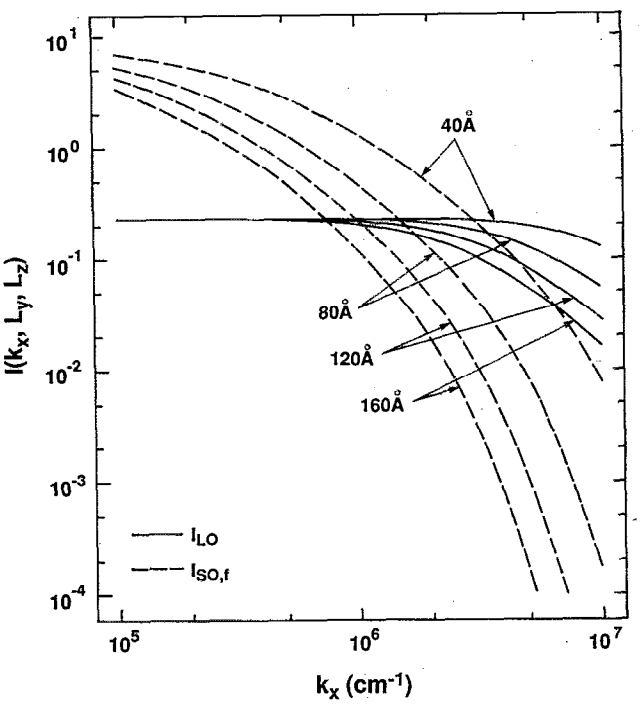


FIG. 3. 1D integral $I(k_x,L_y,L_z)$ for the confined LO-phonon mode (denoted as $I_{LO}$) and the SO-phonon mode in a free-standing quantum wire (denoted as $I_{SO,f}$) as a function of the longitudinal component $k_x$ of phonon wave vector with various wire dimensions ($L_y=L_z$).

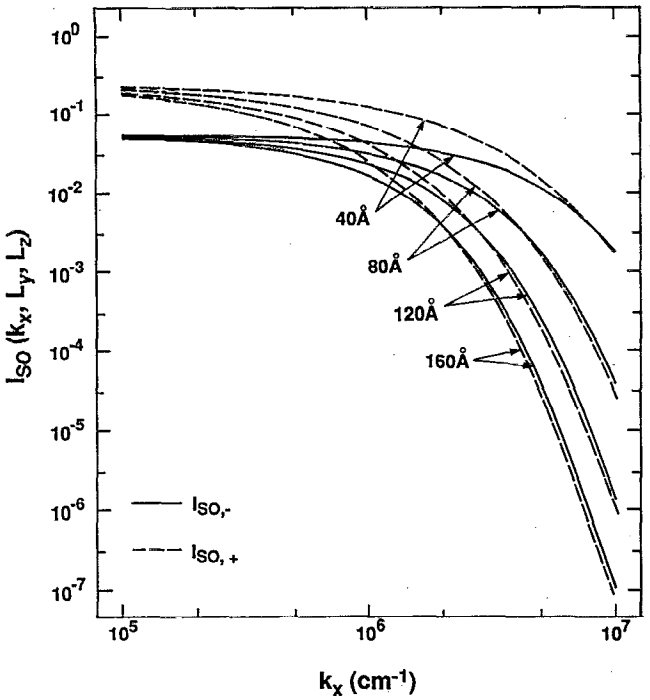


FIG. 4. 1D integral $I_{SO}(k_x, L_y, L_z)$ for the $\omega_{S+}$ SO-phonon mode (denoted as $I_{SO,+}$) and the $\omega_{S-}$ SO-phonon mode (denoted as $I_{SO,-}$) in a GaAs/AlAs quantum wire as a function of the longitudinal component $k_x$ of phonon wave vector with various wire dimensions ($L_y = L_z$).

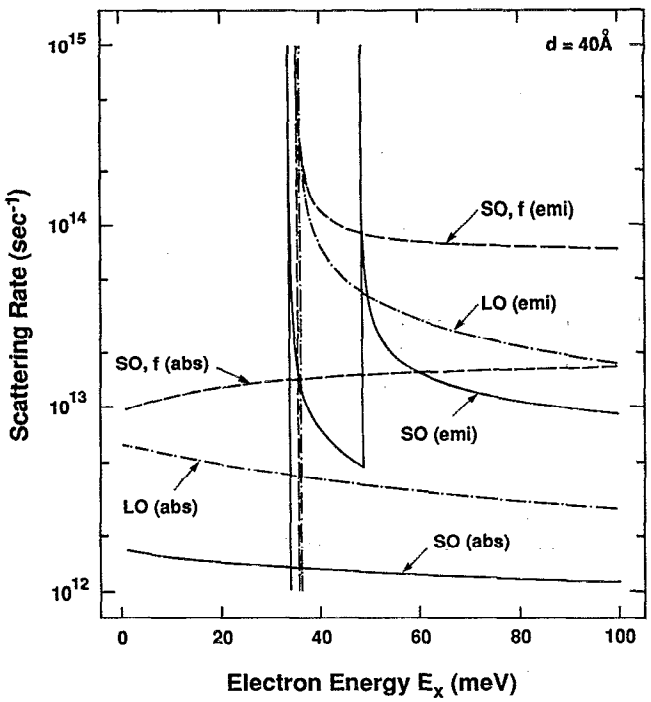


FIG. 5. Scattering rates at 300 K as a function of electron energy $E_x$ in the longitudinal direction. The size of quantum wire, $d$, is 40 Å ($L_y = L_z = d$). The SO-phonon scattering rate is denoted as SO, $f$ for the free-standing quantum wire and as SO for the GaAs/AlAs quantum wire, respectively, while LO represents the rate of electron scattering with confined LO-phonon modes. Phonon emission (absorption) process is represented as emi (abs), respectively.

+ ( − ) modes have AlAs-like (GaAs-like) characteristics, respectively. Considering the functional form of Eq. (30), it is apparent that the comparison between $I_{LO}$ and $I_{SO}$ can give a clear indication on the relative strength of the scattering rates by the LO-phonon and (symmetric) SO-phonon modes. To facilitate such an analysis, Fig. 3 presents $I_{LO}$ from Eq. (23) and $I_{SO}$ for the free-standing wire (denoted as $I_{SO,f}$) as a function of $k_x$, while Fig. 4 depicts $I_{SO}$ for the $\omega_{S+}$ mode ($I_{SO,+}$) and the $\omega_{S-}$ mode ($I_{SO,-}$). As is apparent from the derivation of Eqs. (26)–(28), it is necessary to add the contributions of the $\omega_{S+}$ and $\omega_{S-}$ branches to compute the electron-SO-phonon emission and absorption scattering rates when the quantum wire is embedded in AlAs. The results of Figs. 3 and 4 demonstrate several key points: $I_{SO,f}$ for the free-standing quantum wire is approximately 20 times larger than $I_{LO}$ for small $k_x$ ($\lesssim 10^5$ cm$^{-1}$); $I_{SO,+}$ for the $\omega_{S+}$ mode is dominant over $I_{SO,-}$ for the $\omega_{S-}$ mode for small $k_x$ and; $I_{SO,+}$ is comparable in magnitude to $I_{LO}$ for small $k_x$ but decreases much more rapidly as $k_x$ increases.

As is clear from the previous comparison of Figs. 3 and 4, the scattering of electrons by SO phonons may be of significance in these structures. The relative importance of electron-SO-phonon scattering in rectangular quantum wires (in our case $L_y = L_z = d$) is made transparent by using $I_{LO}$ and $I_{SO}$ to compute the scattering rates for various values of the electron energy $E_x$ and the wire dimension $d$. The SO-phonon and LO-phonon scattering rates versus $E_x$ at 300 K are given in Fig. 5 with $d = 40$ Å. Due to the 1D nature of the electronic density of states, the scattering rates increase abruptly to infinity at the onset of emission processes and then gradually decrease. For the SO-phonon modes in the GaAs/AlAs structure (denoted as SO in Fig. 5), the emission rate exhibits two peaks as a result of the two characteristic phonon branches ($\omega_{S+}$ and $\omega_{S-}$). An important point to note in this figure is that the SO-phonon processes in the free-standing wire (denoted as SO, $f$) dominate over the LO-phonon processes (denoted as LO) throughout the values of $E_x$, while in the GaAs/AlAs structure the scattering rates by SO phonons are smaller than those by LO phonons except for a narrow range of $E_x$ (due to the 1D electronic density of states). Even in the GaAs/AlAs structure, however, the SO-phonon emission rates become comparable to the LO-phonon emission rates when $E_x > \hbar\omega_{S+}$. These results can be readily understood from the magnitude of $I_{LO}$, $I_{SO,f}$, $I_{SO,-}$, and $I_{SO,+}$ as discussed previously. The LO-phonon scattering rate of Fig. 5 is similar in functional form to the results of Leburton.[4]

Figures 6 and 7 illustrate how the SO-phonon and LO-phonon scattering rates depend on $d$ at $E_x = 45$ meV and 100 meV, respectively. The particular values of $E_x$ are chosen to appropriately reflect the two-mode nature of the SO-phonon modes in the quantum wire surrounded by AlAs. In Fig. 6, it is observed that the SO-phonon emission rate in the GaAs/AlAs structure is always smaller than the LO-phonon emission rate as expected from the discussion of Fig. 5. In the free-standing wire, however, SO-phonon emission dominates over the LO-phonon emission for val-

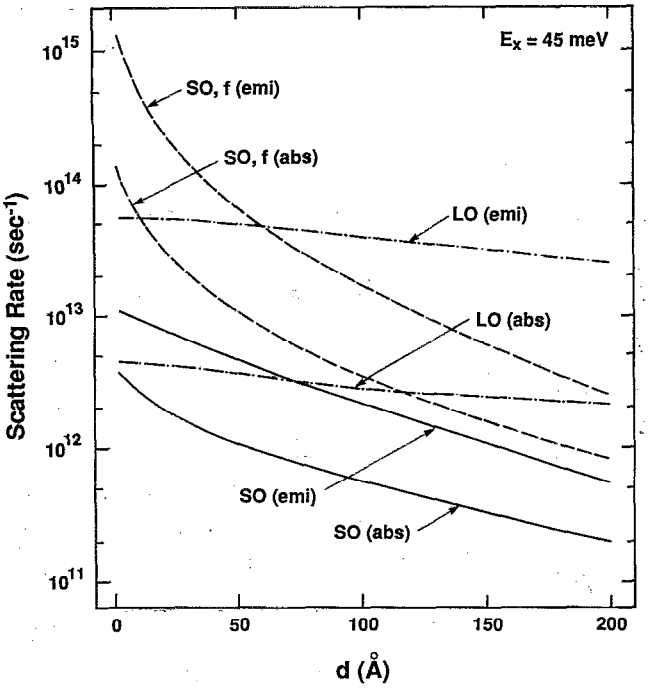


FIG. 6. Scattering rates at $E_x = 45$ meV as a function of quantum wire dimension, $d$ ( $= L_y = L_z$). All of the notations are the same as Fig. 5.

ues of $d$ less than about 60 Å. As the electron energy $E_x$ increases and the emission of the $\omega_{S+}$ mode becomes permissible, the relative strength of SO-phonon modes increase compared to the LO-phonon modes both in the free-standing wire and in the GaAs/AlAs quantum-wire structure. As a result, at $E_x = 100$ meV the cross-over between the SO-phonon and LO-phonon emission rates in the free-standing wire occurs at a larger $d$ ($\sim 140$ Å). At the same time, the SO-phonon modes in the GaAs/AlAs quantum wire also increases rapidly and becomes comparable to (or, even larger than) the LO-phonon mode as the wire dimension, $d$, decreases. It is instructive to note that the quantum wires free-standing in vacuum always exhibit far stronger SO-phonon modes than those embedded in polar semiconductors. This is obvious from Eq. (14). The free-standing wire has no "leakage" of SO modes (i.e., no polarization) in the surrounding environment (i.e., $\epsilon_2 = 1$), while the strength of SO modes outside the quantum wire is significant when embedded in a polar semiconductor (for example, AlAs). Use of more realistic electronic states for the quantum wire (with tails) would enhance the scattering rates by SO-phonon modes calculated in the embedded structures. Based on the macroscopic dielectric continuum model, it is then clear that SO-phonon scattering will be a significant energy loss mechanism in GaAs quantum wires and in mesoscopic structures with ultrasmall dimensions.

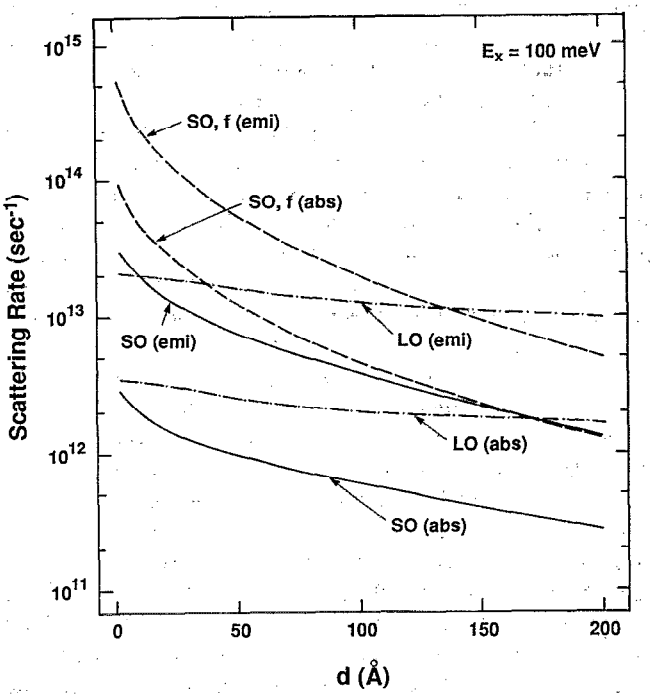


FIG. 7. Scattering rates at $E_x = 100$ meV as a function of quantum wire dimension, $d$ ( $= L_y = L_z$). All of the notations are the same as Figs. 5 and 6.

## V. CONCLUSION

Based on the macroscopic dielectric continuum model, we have derived the Hamiltonian describing the interaction of both confined LO and SO phonons with charge carriers in a rectangular quantum wire where electron and phonon confinement occurs in two of the three spatial dimensions. The interaction Hamiltonian is used to calculate the electron-optical-phonon scattering rates in a GaAs square quantum wire with two surrounding materials: (1) free-standing in vacuum and (2) embedded in AlAs. Our results lead to new predictions for electron-optical-phonon scattering rates in confined quantum structures. Furthermore, within the macroscopic dielectric continuum approximation, it is observed that as the dimensions of the quantum-wire structures decrease, electron-SO-phonon scattering can be significant and may dominate over (or, at least, be comparable to) the electron-LO-phonon scattering. It is anticipated that SO-phonon scattering will play an important role in mesoscale devices where it is of major importance to engineer ultrasmall devices so that the phase coherence of de Broglie wave is retained.

## ACKNOWLEDGMENTS

The authors would like to thank Dr. G. J. Iafrate, Professor M. A. Littlejohn, and Dr. J. Mink for helpful discussions. This work is, in part, supported by the Office of Naval Research under Grant N00014-90-J-1835 and the U. S. Army Research Office under Grant DAAL03-89-D-0003-05.

[1] M. Tsuchiya, J. M. Gaines, R. H. Yan, R. J. Simes, P. O. Holtz, L. A. Coldren, and P. M. Petroff, Phys. Rev. Lett. **62**, 466 (1989); J. Vac. Sci. Technol. B **7**, 315 (1989).

[2] M. Watt, C. M. Sotomayor Torres, H. E. G. Arnot, and S. P. Beaumont, Semicond. Sci. Technol. **5**, 285 (1990).

[3] G. Fasol, M. Tanaka, H. Sakaki, and Y. Horikosh, Phys. Rev. B **38**, 6056 (1988).
[4] J. P. Leburton, J. Appl. Phys. **56**, 2850 (1984); S. Briggs and J. P. Leburton, Phys. Rev. B **38**, 8163 (1988); S. Briggs, D. Jovanovic, and J. P. Leburton, Appl. Phys. Lett. **54**, 2012 (1989).
[5] F. Sols, M. Macucci, U. Ravaioli, and K. Hess, Appl. Phys. Lett. **54**, 350 (1989); F. Sols and M. Macucci, Phys. Rev. B **41**, 11887 (1990).
[6] H. Sakaki, Jpn. J. Appl. Phys. **28**, L314 (1989).
[7] J. J. Licari and R. Evrard, Phys. Rev. B **15**, 2254 (1977).
[8] N. Mori and T. Ando, Phys. Rev. B **40**, 6175 (1989).
[9] M. A. Stroscio, Phys. Rev. B **40**, 6428 (1989).
[10] See, for example, A. K. Sood, J. Menendez, M. Cardona, and K. Ploog, Phys. Rev. Lett. **54**, 2111 (1985); **56**, 1753 (1986).
[11] M. A. Stroscio, K. W. Kim, M. A. Littlejohn, and H. Chuang, Phys. Rev. B **42**, 1488 (1990).
[12] E. A. J. Marcatili, Bell System Tech. J. **48**, 2071 (1969).
[13] J. E. Goell, Bell System Tech. J. **48**, 2133 (1969).
[14] L. Wendler, Phys. Status Solidi B **129**, 513 (1985).
[15] R. Chen, D. L. Lin, and T. F. George, Phys. Rev. B **41**, 1435 (1990).